THE AMERICAN SOCIETY OF MECHANICAL ENGINEERS
345 E. 47th St., New York, N.Y. 10017

98-GT-188

ENDWALL BLOCKAGE IN AXIAL COMPRESSORS

S. Arif Khalid
Allison Advanced Development Company
Indianapolis, IN 46206 USA

Amrit S. Khalsa
Khalsa International Industries and Trades
Eugene, OR 97402 USA

Ian A. Waitz, Choon S. Tan
Massachusetts Institute of Technology
Cambridge, MA 02139 USA

Edward M. Greitzer*
United Technologies Research Center
E. Hartford, CT 06108 USA

Nicholas A. Cumpsty
Cambridge University
Cambridge, CB3 ODY UK

John J. Adamczyk
NASA Lewis Research Center
Cleveland, OH 44135

Frank E. Marble
California Institute of Technology
Pasadena, CA 91125

ABSTRACT

This paper presents a new methodology for quantifying compressor endwall blockage and an approach, using this quantification, for defining the links between design parameters, flow conditions, and the growth of blockage due to tip clearance flow. Numerical simulations, measurements in a low speed compressor, and measurements in a wind tunnel designed to simulate a compressor clearance flow are used to assess the approach. The analysis thus developed allows predictions of endwall blockage associated with variations in tip clearance, blade stagger angle, inlet boundary layer thickness, loading level, loading profile, solidity and clearance jet total pressure. The estimates provided by this simplified method capture the trends in blockage with changes in design parameters to within 10%. More importantly, however, the method provides physical insight into, and thus guidance for control of, the flow features and phenomena responsible for compressor endwall blockage generation.

NOMENCLATURE

A	area
c	chord length
CP_S	static pressure coefficient, $\dfrac{\overline{P_{S,exit}}^a - \overline{P_{S,in}}^a}{Q_{in}}$
CP_T	defect total pressure coefficient, $\dfrac{\overline{P_{T,exit}}^a - \overline{P_{T,in}}^a}{Q_{in}}$
C_x	axial velocity
h	blade height
P	pressure
Q	dynamic head
s	blade spacing
u	velocity component
U	velocity magnitude
α_0	ratio of defect velocity to freestream velocity
β_e	relative flow exit angle
σ	solidity = c/s
ρ	density
τ	tip clearance height
δ^*	displacement thickness

Subscripts and Superscripts

a	area-weighted average
b	blocked
$edge$	edge of blockage area
ex	exit
in	inlet
m	mainflow direction
mid	midspan
S	static
T	total
1	upstream, inlet
2	downstream, exit

1.0 INTRODUCTION

It has long been known that the flow in the endwall region of an axial compressor has a strong influence on overall performance and stability. For example, Wisler (1985) suggests that more than half the loss in an axial compressor is associated with the flow in the endwall region. The large amount of data presented by Koch (1981) also emphasizes the detrimental effect of increasing tip clearance on the maximum pressure rise obtainable within a blade passage.

* On leave from Massachusetts Institute of Technology

Presented at the International Gas Turbine & Aeroengine Congress & Exhibition
Stockholm, Sweden — June 2–June 5, 1998
This paper has been accepted for publication in the Transactions of the ASME
Discussion of it will be accepted at ASME Headquarters until September 30, 1998

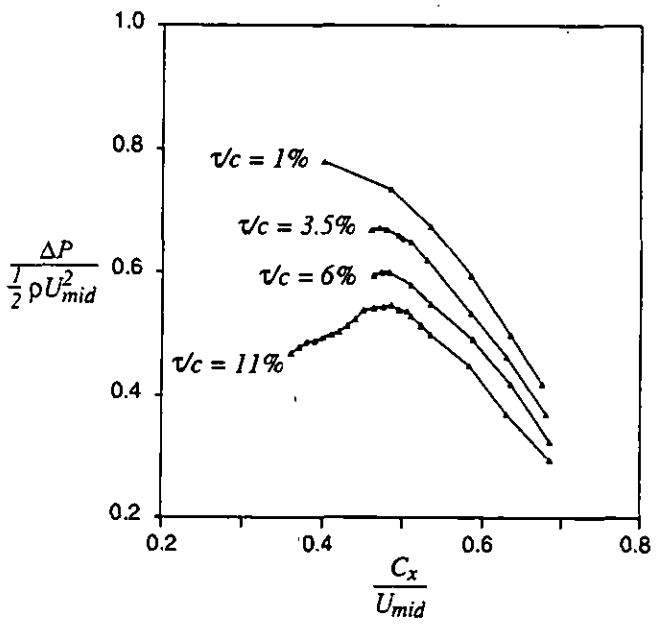

Figure 1: Compressor characteristics for various tip clearance sizes from Smith and Cumpsty (1984).

Figure 1, adapted from Smith and Cumpsty (1984), illustrates the effects of tip clearance on pressure rise capability for a low speed rotor. As the mass flow is decreased the pressure rise coefficient increases to a peak and then declines. The peaking of the characteristic is due to the reduction in blade passage exit effective flow area which can be associated with either the formation of regions of substantial velocity defect or with deviation. Of these, it is the former, commonly referred to as "blockage", which appears to be more important. Similar effects are observed in transonic fans as illustrated by Suder (1997) who attributed endwall blockage primarily to shock/tip leakage vortex interaction.

Further, the present understanding of rotating stall in axial compressors traces a clear line between one route to stall inception and peaking over of the pressure rise characteristic. In compressors in which flow in the tip region is primarily responsible for blockage growth, rotating stall onset is thus linked to phenomena associated with clearance flow. There is therefore strong motivation to understand the key features of the endwall flow field and to develop techniques to modify it. However, in spite of the importance of the endwall flow field in determining the pressure rise capabilities of axial compressors (as well as the existence of many experimental, analytical and, most recently, computational investigations of this topic), complete explanations of the mechanisms through which the endwall flow degrades compressor performance still do not exist. Empirical correlations are typically employed in the design process, with different organizations developing these from quite different physical viewpoints (Koch, 1981; Schweitzer and Garberoglio, 1984).

1.1 Problem Statement

The primary issues addressed in this paper are:

1) The development of a procedure to quantify compressor endwall blockage.
2) The definition of a simplified, physically-based model for endwall blockage.
3) The determination of the relative sensitivity of blockage to various compressor design parameters.
4) The development of quantitative criteria for blockage management.

1.2 Approach

The approach taken in this paper can be stated as follows. A basic premise (which is shown in the paper) is that many of the features of compressor tip clearance flows can be captured by three-dimensional computations that are in widespread usage. In spite of the computational capability, however, links between design parameters, flow conditions, and compressor endwall blockage are typically still dealt with on a configuration-specific basis. More precisely, there appears to be no unified framework that not only captures the underlying fluid dynamics that define these links, but also allows one to view them on a more global basis. Describing such a framework is the central objective of this paper. The framework is intended to *complement* computations, enabling the development of physically-based guidelines for the control of tip leakage flows.

In this context, both computational and experimenal results were examined to address the issues listed above. The computations, which allowed detailed flow field investigation, were carried out using the three-dimensional Reynolds-averaged Navier-Stokes solver described by Adamczyk *et al.* (1989). Wind tunnel experiments designed to simulate a compressor endwall flow were used to isolate key design parameters. Data from a low speed compressor was used to support and confirm the computations and extend the parameter space studied.

Computations were performed on three blade geometries: the cantilevered stator described by Johnson and Greitzer (1987), the low speed General Electric E^3 Rotor B described by Wisler (1977) and Wisler (1981), and the transonic fan, NASA Lewis Rotor 67, whose performance has been reported by Strazisar *et al.*, (1989). The cases cover a range of flow and geometric parameters relevant for the design of modern, efficient compressors. Data from the experiments was used to corroborate the computational results and ensure that the computations captured the physical phenomena examined. The low speed compressor experiments were carried out at the Whittle Laboratory. Two clearance levels and five loading levels were tested, covering a range of flow conditions similar to the computations. The experiments conducted using this rig were described in detail by Khalsa (1996).

The scope of the paper is as follows. Section 2 describes the method for quantification of blockage in compressors. Section 3 then presents simplified mechanistic arguments about the behavior of a velocity defect in a pressure gradient, which will be later shown to apply directly to the description of compressor

blockage formation. Section 4 then shows a number of parametric trends of endwall blockage, using experiments as well as computations. Following from this, Section 5 integrates the ideas of Section 3 with the computations and data of Section 4 to develop a basic analysis for estimating blockage. Applications and parametric trends are given in Section 6.

2.0 QUANTIFICATION OF ENDWALL BLOCKAGE

The term "blockage", which is widely used in discussions regarding axial compressor flows, generally refers to the reduction in effective freestream or core flow area due to local velocity defects, analagous to the displacement thickness associated with boundary layers. Past assessments of blockage have, for the most part, been limited to qualitative descriptions regarding the size and severity of the apparent nonuniformity or velocity defect present in the flow, *e.g.*, Smith and Cumpsty (1984) and Crook *et al.* (1993). Some techniques to quantify blockage or displacement thickness have been suggested, notably that of Smith (1970) (see also Dring, 1984), but none have linked the nonuniformity in the local defect region to the freestream or "core" region velocity and thus, to the pressure rise, in a rigorous manner.

To identify trends in blockage, as well as to help in understanding the underlying mechanisms that affect the generation of blockage, a quantitative means of assessment is required. In this section, we present a method for defining blockage in axial compressors and apply the method to a low speed rotor and a transonic fan. The resulting blockage values are used to illustrate the role of clearance in blockage growth. The description given here represents an overview of the method; a more detailed description is presented by Khalid (1995).

The concept of a blocked area is similar to a boundary layer displacement thickness, as illustrated in Fig. 2. The challenges associated with defining the blockage in a compressor blade row flow field are that the flow is multi-directional, and the freestream is non-uniform. These aspects raise two questions: (1) What velocity component is relevant for defining blockage? and (2) How can the edge of the defect region be identified given the presence of strong gradients in freestream flow properties?

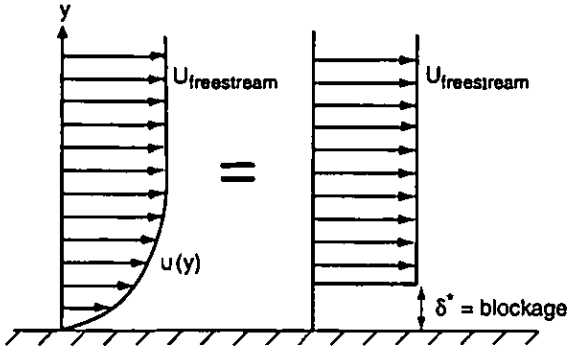

Figure 2: Blockage schematic.

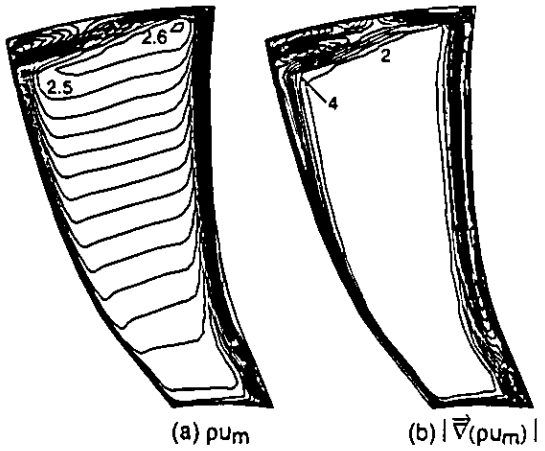

Figure 3: Example of blockage region definition using velocity gradient.

In addressing these questions, we note some features that are common for many situations of technological interest. First, the compressor freestream or core flow has an identifiable direction which may be called the throughflow or *mainflow* direction. This mainflow direction can be used to select the velocity component to use in the blockage definition. Second, although the core flow may be non-uniform, we can distinguish between this region and that existing near endwalls or blades because the *gradients* in flow properties in wall regions are significantly greater than those in the core region. This aspect can thus be used to identify the edge of the defect region.

An expression for blocked area applicable for the flow within a compressor blade row is

$$A_b \equiv \iint \left(1 - \frac{\rho u_m}{\rho_{edge} U_{edge}}\right) \cdot dA \qquad (1)$$

where the integral is taken over the defect region. This is formally the same as the definition of displacement thickness but two clarifying statements need to be made. First, the edge criterion is based on $\bar{\nabla}(\rho u_m)$, where u_m is the component of velocity resolved in the mainflow direction. Specifically, the edge of the defect region is defined by the magnitude of the vector formed by the two gradient components lying in the plane of the integration. Thus, to calculate blockage in an axial plane, the magnitude of the vector formed by the radial and tangential components of $\bar{\nabla}(\rho u_m)$ is used to define the edge. The value selected as the edge criterion is the minimum value not found in the core region. As is shown below, this cutoff value is quite distinct even for the highly non-uniform core regions representative of low hub-tip ratio fans. The edge velocity and density (U_{edge} and ρ_{edge}, respectively) in Eq. (1) are the values along the edge of the blockage region nearest to the local area over which the integration is taken.

Figure 3 shows contours of ρu_m and the magnitude of

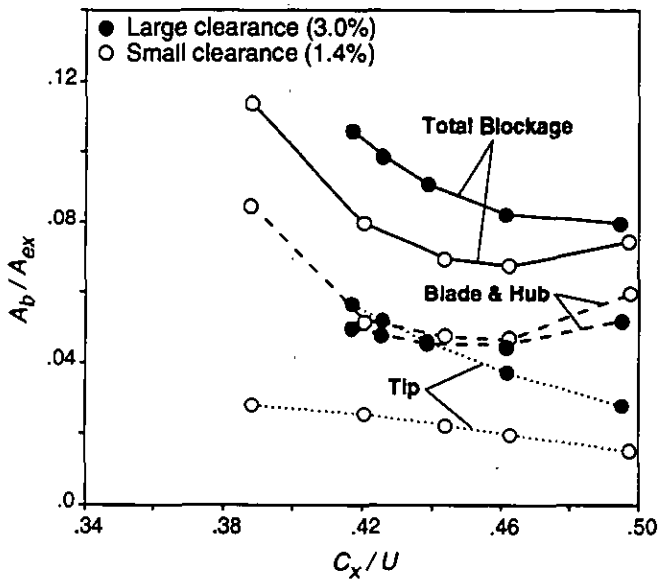

Figure 4: Blockage versus mass flux.

$\bar{V}(\rho u_m)$ for a transonic fan with a hub-to-tip ratio of 0.67, normalized using the inlet average density, axial velocity, and tip chord. Although the freestream velocity varies by more than a factor of two, the gradient magnitude provides an unambiguous indication of the defect region. Further, the defect area over which the blockage integration is performed is relatively insensitive to the precise value selected (*e.g.*, 2, 3, or 4) as the edge criterion.

To illustrate the trends with operating condition and clearance, trailing edge blockage values calculated in this manner for the low speed rotor are plotted as a function of compressor flow coefficient in Fig. 4. In the simulations, the flow coefficient was reduced until a converged solution could no longer be obtained. The open and filled symbols correspond to 1.4% and 3.0% clearance, respectively. The solid curves represent blockage calculated over the full span, while the dotted curves represent the blockage contribution associated with the tip clearance, and the dashed curves represent the contribution of the blade and hub.

For the smaller clearance, comparison of total blockage and tip clearance-related blockage indicates that little of the growth in blockage with increased loading is due to clearance flow. The blockage increase with loading is primarily due to growth of the suction surface boundary layer and the development of endwall-suction surface corner separation as the flow coefficient is reduced.

For the larger clearance, the tip clearance-related blockage, and the total blockage are larger than for the smaller clearance. Furthermore, with 3.0% clearance the growth in clearance-related blockage with loading is almost entirely responsible for the growth in total blockage. For this rotor, increasing the clearance changes the region most responsible for limiting the pressure rise from the blade suction surface and the endwall corner at small clearance to the tip region at large clearance.

3.0 NORMALIZATION AND PARAMETERIZATION OF BLOCKAGE

As background for discussing the endwall blockage trends and to motivate the parameters we use to collapse blockage data onto a single trend line, we first present a simplified description of the behavior of velocity defects passing through a pressure difference. We consider a velocity defect passing through a pressure rise in a quasi-one-dimensional, inviscid, incompressible flow, as indicated in Fig. 5. The initial normalized velocity in the defect has a magnitude $\alpha_0 = u_1/U_1$ and an extent A_1. Of interest is the effective blocked area, A_{b2}, at station 2, after the pressure rise, where A_{b2} is defined as

$$A_{b_2} \equiv \left(1 - \frac{u_2}{U_2}\right) \cdot A_2 \qquad (2)$$

Using continuity and Bernoulli's equation gives an expression for A_{b2}/A_1,

$$\frac{A_{b_2}}{A_1} = \alpha_0 \left[\left(\alpha_0^2 - CP_S\right)^{-1/2} - \left(1 - CP_S\right)^{-1/2} \right] \qquad (3)$$

where

$$CP_S \equiv \frac{\Delta P_S}{\frac{1}{2}\rho U_1^2}$$

is a static pressure rise coefficient.

Equation (3) shows that exit blockage is a function of both the initial velocity defect, α_0, and the non-dimensional static pressure rise, CP_S. This is illustrated in Fig. 6a, which shows A_{b2}/A_1 versus CP_S for four different values of α_0 spanning the values observed in the flow fields examined in this study. Figure 6a also shows that each curve possesses an asymptotic behavior in that there is a critical value of CP_S, dependent on the initial defect, where the blockage increases rapidly; Eq. (3) indicates this occurs at a pressure rise coefficient equal to α_0^2.

These statements may be put in a form that is more useful for the present problem if we work in terms of total pressure in the defect rather than α_0. We thus define an exit plane total pressure coefficient:

$$CP_T \equiv \frac{P_{T,defect} - P_{T,freestream}}{Q_{in,freestream}} = \alpha_0^2 - 1 < 0 \qquad (4)$$

With this definition, Eq. (3) can be rewritten as

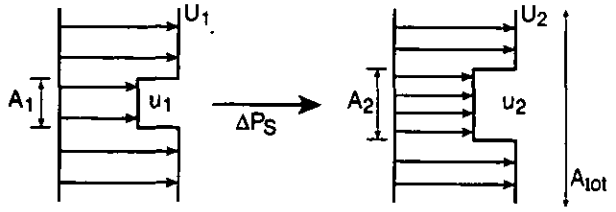

Figure 5: Schematic of one-dimensional blockage description.

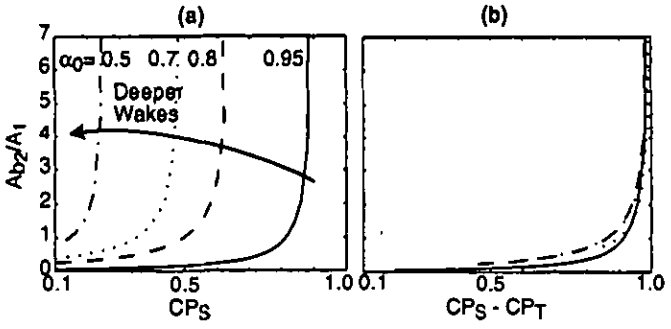

Figure 6: One-dimensional blockage results: (a) Blockage as a function of CP_S, (b) Blockage as a function of CP_S-CP_T.

$$\frac{A_{b_2}}{A_1} = \sqrt{1+CP_T}\left\{\left[1-(CP_S-CP_T)\right]^{-1/2}-(1-CP_S)^{-1/2}\right\} \quad (5)$$

An advantage of writing the equation this way is that the asymptote in the blockage occurs when CP_S - CP_T = 1 for all initial defects. One view of this is that what we will term the loading parameter, CP_S - CP_T, is related to the defect dynamic head as follows:

$$CP_S - CP_T = 1 - \frac{Q_{defect}}{Q_{in}} = 1 - \frac{u_2^2}{U_{in}^2} \quad (6)$$

Blockage will asymptote when the defect velocity decelerates to zero, which will occur when the loading parameter equals one.

Figure 6b shows how different initial conditions are nearly collapsed to a single trend when blockage is plotted against this loading parameter CP_S - CP_T. Thus, although in general exit blockage depends on both CP_S and CP_T independently, Fig. 6 demonstrates that, within the range of initial defects and static pressure rises examined in this study, the primary trend is well-captured by the dependence on CP_S - CP_T only.

We can now link the CP_S and CP_T parameters in the simplified one-dimensional (1-D) description to a compressor tip leakage flow by defining the initial conditions as leakage jet, mass flux-weighted averages along the blade chord, and the final conditions as averages over the blockage region (as defined in Section 2) in the blade passage exit plane. In Section 4, we show that blockage estimates obtained from experiments and numerical simulations of a range of compressor geometries collapse onto a single trend line when the data is characterized in this manner. A single limiting value of the loading parameter, CP_S - CP_T, is thus found to describe the experimental limiting pressure rise condition. This concept, plus the quantification of blockage, will be seen to enable estimation of clearance blockage growth in a wide range of situations.

4.0 EXPERIMENTAL DATA AND NUMERICAL SIMULATIONS

In this section we present blockage estimates obtained from low-speed compressor tests, Navier-Stokes computations, and tests in a wind tunnel model designed to capture the essential elements of tip leakage flows. Descriptions of each of these tools are provided and the blockage estimates are presented using the framework discussed in Section 3.

4.1 Low Speed Compressor Tests

Tests were performed in the Deverson low speed compressor at the Whittle Laboratory of Cambridge University. The facility consisted of a calibrated bellmouth inlet with honeycomb flow straighteners, casing boundary layer thickening tabs, inlet guide vanes, a rotor (51 blades) and stator (49 blades) with a hub-to-tip ratio of 0.8, and an auxiliary exhaust fan. The inlet guide vanes were 3.2 rotor chords upstream of the rotor leading edge, imparting swirl to the flow, but allowing the circumferential non-uniformities due to inlet guide vane (IGV) wakes to mix out. The rotor and stator blading is representative of a modern high pressure compressor stage, with controlled diffusion airfoils. The primary features of the blading are summarized in Table 1.

Table 1: Low Speed Compressor Rig Blading Parameters

Tip chord	119 mm
Tip solidity	1.26
Hub/tip ratio	0.80
Tip camber	25.4°
Inlet δ^*/τ	2.0
Design C_x/U_{tip}	0.63

All data were taken at a rotor tip speed of 32 m/s, giving a Reynolds number based on tip speed and chord of approximately 2.5×10^5.

Data were collected primarily with a slant hotwire traversed radially 15% chord downstream of the rotor trailing edge. At each radial location phase-locked measurements were taken and ensemble-averaged for 8 different wire orientations. The data were used to calculate each of the three rotor exit velocity components with 27 data points in the radial direction and 39 across the blade pitch. The error of the rotor exit plane velocities was less than ±5% with 95% confidence (Khalsa, 1996).

Trailing edge velocity data were taken at a number of points along a speedline. Speedlines were run for two stagger angles (40.5° and 44.7°) and two clearance levels (τ/c = 1.24% and 3%). For the increased clearance tests, three blades were cropped to increase their clearance. The circumferential non-uniformity in clearance was accounted for in the data reduction using the theory of Horlock and Greitzer (1983) to find the circumferential redistribution of flow coefficient for a given circumferential tip clearance variation. Using this analysis, the local flow coefficient for the large clearance blades was estimated to be approximately 8% less than the mean flow coefficient.

Representative contour plots of the relative velocity magnitude normalized by midspan blade speed are shown in Fig. 7 for

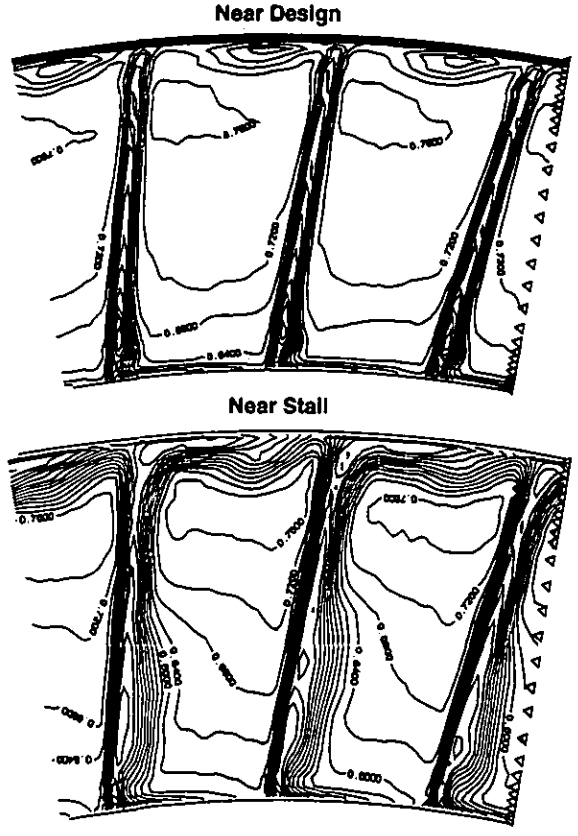

Figure 7: Relative velocity, w/U_{mid}, contours from rotating rig at trailing edge +15% chord.

the datum stagger and clearance geometry at two flow conditions. The triangles along the right hand edge indicate the radial measurement locations. For both plots the contour intervals are 0.04 w/U_{mid}, and the direction of blade rotation is right to left.

Blockage was calculated at each flow condition using the technique described above, and was normalized by clearance area (τc) and multiplied by the cosine of the exit flow angle. The loading parameter ($CP_S - CP_T$) was calculated using a mass-average of the local loading parameter $(CP_S - CP_T)_{local}$ corresponding to each chordwise station along the blade:

$$(CP_S - CP_T)_{local} = \left[\frac{\overline{P_{S,exit}}^{a} - P_{S,local,suction\ side}}{Q_{local,suction\ side}}\right] - \left[\frac{\overline{P_{T,exit}}^{a} - P_{T,inlet\ freestream}}{Q_{local,suction\ side}}\right]$$

where $\overline{(\,)}^{a}$ denotes an area-average over the blockage region (as defined in Section 2.0). The inlet freestream conditions (used also for Q_{local}) were calculated from the experimental data using an area-average upstream of the blade row over a region extending approximately 10τ outside of the endwall boundary layer.

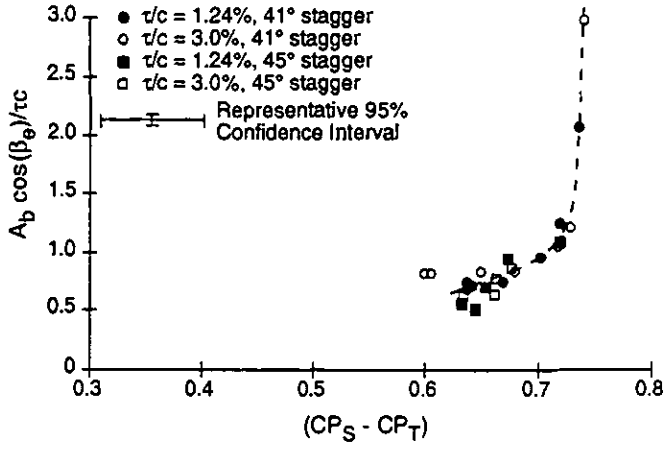

Figure 8: Blockage versus loading parameter from rotating rig experiments, two clearance heights, two stagger angles.

A plot of blockage versus loading parameter for all the data points taken is shown in Fig. 8. The highest loading points were at "near-stall" conditions (flow coefficients approximately 0.03 C_x/U_{tip} above the onset of rotating stall). The most evident aspect of Fig. 8 is the asymptotic trend similar to that seen in the one-dimensional description given in Section 3. The primary difference between the data and the one-dimensional results is the location of the asymptote which occurs at a limiting loading parameter of approximately 0.72 in the data rather than at a value of 1.0. The difference is due to the averaging used to calculate the local loading parameter. Each chordwise section of the clearance jet undergoes a different static pressure rise[1] and a different amount of loss, and the blockage will reach its asymptote when the loading parameter of a *local* streamtube approaches unity.

4.2 Wind Tunnel Simulation

Marble suggested that the key feature of the flows of interest was the growth of blockage due to the tip leakage as the clearance vortex negotiated the blade row pressure rise. Based on this idea, an experiment was set up to enable the flow field to be examined in a way that allowed more control over flow conditions than can be achieved in the rotating rig.

In this experiment, the compressor tip clearance flow was represented by an axial slot jet entering a freestream within an adverse pressure gradient, as shown schematically in Fig. 9. The slot produces a symmetric vortex pair, similar to the wall-bounded single vortex with an image vortex set by the boundary conditions on the casing wall. The advantage of capturing the vortex/image-vortex interaction with a vortex pair is that this implementation, where the symmetry plane between the two vortices

[1] The exit pressure is essentially the same for each streamtube, but the initial pressure, the pressure along the blade suction surface, has significant variations along the chord.

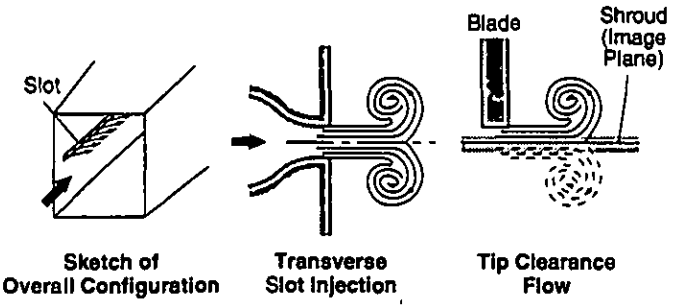

Figure 9: Wind tunnel concept.

represents the casing boundary (Fig. 9), simulates the high total pressure at the casing boundary that exists in a compressor rotor due to the relative motion of the wall without the experimental complications of a moving wall.

The wind tunnel test section was constructed to produce an adverse pressure gradient representative of that found in an axial compressor, with simultaneous turning and diffusion, a local minimum in pressure as the flow accelerates around a bend, and then an increase in pressure. A schematic of the tunnel is shown in Fig. 10. The curved wall in the test section is representative of the suction surface of a rotor blade, and it is through this wall that the leakage jet was injected.

Because of the strong adverse pressure gradients along the curved wall which correspond to the blade suction surface, several bleeds were located to prevent boundary layer separation. The simulation of the tip leakage flow was produced by blowing from a 1/4 inch slot located in the center of the tunnel as shown in the three-dimensional view of the tunnel in Fig. 10. A chamber which could be pressurized independently of the main tunnel was used to create the clearance jet. Immediately behind the slot inside the pressurized chamber was a set of vanes (not shown) that turned the flow in a prescribed direction. A series of screens was placed upstream of the vanes to condition the flow. Based on data on clearance flow angles (Storer and Cumpsty, 1991), two sets of turning vanes were used, creating jets which were 41° and 54° from the local freestream direction, uniform along the chord.

The primary diagnostic tool for the wind tunnel tests was a seven hole pneumatic probe with 0.10″ diameter tip. Having seven measurements allows for the five steady flow quantities of interest, three velocity components, static pressure, and total pressure, to be measured even when the flow is separated over part of the probe tip. The probe could operate with flow angles up to 80 degrees from the probe axis. A description of the probe is given in Rediniotis *et al.* (1993). The probe measured dynamic head to within 1%, and both pitch and yaw angles to within 0.7°. These uncertainties result in uncertainty in the normalized blockage of ±0.14 and uncertainty in the loading parameter of ±0.035, both with 95% confidence. A full description of the experiments can be found in Khalsa (1996).

The wind tunnel experiment neglects effects such as the variation in leakage angle along the chord, and the presence of an inlet casing boundary layer. Estimates of the effects on blockage of these flow features, however, indicate that the wind tunnel should adequately capture the parametric trends of endwall blockage (Khalsa, 1996).

The experimental results from the wind tunnel and from the rotating rig are shown in Fig. 11. The blockage trends from the wind tunnel simulation match the trends observed in the rotating rig to within 7% of the inlet dynamic head when viewed in terms of the limiting loading parameter. This not only argues for the use of the wind tunnel to explore the parameter space of interest, but lends additional support to the use of the parameter $CP_S - CP_T$ as a relevant descriptor of blockage formation. Further results from this facility will be presented in Section 6.

4.3 Navier-Stokes Computations

The three-dimensional Navier-Stokes flow solver used was developed by Adamczyk *et al.* (1989). The equations of motion

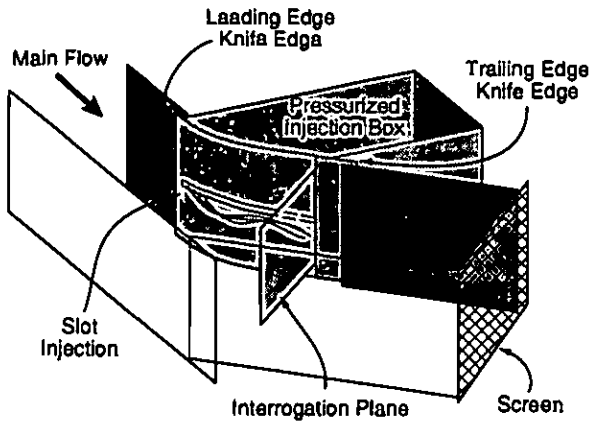

Figure 10: Three dimensional schematic of wind tunnel test section.

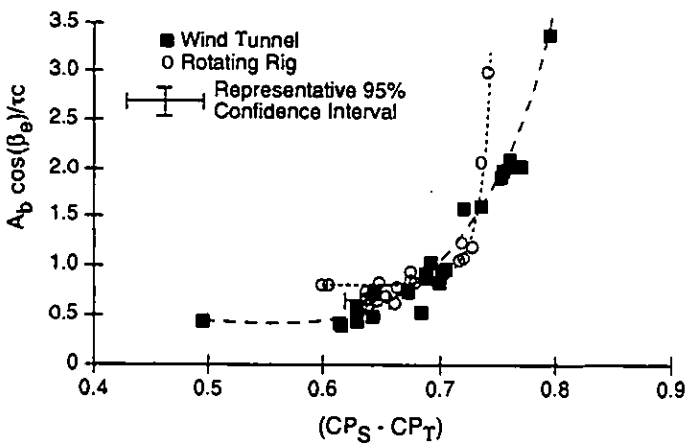

Figure 11: Comparison between wind tunnel and rotating rig.

are Reynolds-averaged, and discretized in cylindrical coordinates. The turbulent viscosity was modeled using the Baldwin and Lomax (1978) mixing length model, and both second and fourth order artificial viscosity were used in the inviscid regions of the flow field to maintain stability (*i.e.* artificial viscosity was not used in the boundary layer). The flow solver is not well-suited for very low Mach numbers, so solutions were obtained with an inlet Mach number of 0.3, approximately double the experimental Mach number. Numerical results for two different grid densitites and for levels of turbulent viscosity that differed by a factor of 10 were compared to experimental data by Khalid (1995). The grid density and turbulent viscosity that produced the best agreement with the experimental data were used for the studies presented in this paper.

The clearance gap was not gridded in these solutions. The model suggested by Kirtley *et al.* (1990) was used, in which the region from blade tip to casing is specified as periodic from pressure side to suction side of the passage. Khalid (1995) explicitly examined this modeling assumption and concluded that the clearance related blockage was adequately captured. He also compared the discharge coefficient from the numerical solutions to experiment and determined that the physical clearance is approximately equal to the specified computational clearance.

Two blade rows were examined, a cantilevered stator and a low speed rotor. The stator blades were cantilevered from the casing and had a rotating hub, as described in the experimental study of Johnson and Greitzer (1987). Simulations were carried out for two tip clearances, 1.75% and 3.5% of chord. Loading was specified by an inlet flow angle distribution, with the baseline case using experimental near-stall data. This flow angle was increased uniformly over the span to obtain solutions at a number of mass flows, three for the small clearance case, and five for the large clearance geometry.

The geometry of the low speed rotor was the General Electric E^3 Rotor B, described in detail by Wisler (1977). Solutions were computed for two clearance heights, 1.4% and 3.0% of chord. Loading was varied by specifying the hub static pressure at the exit of the computational domain. Inlet data from experiments were used for the datum solutions. In addition, solutions were also obtained for 50% increased solidity. Solutions were computed for a thickened inlet boundary layer (axial displacement thickness three times the datum) and no inlet boundary layer (axial velocity profile uniform to the endwall).

Table 2: Geometric Parameters for Computed Solutions

Blade	τ/c	c/s	h/c	Stagger	Camber	Inlet δ^*/τ
LSS	1.75	1.2	1.9	45°	30°	2.8
"	3.5	1.2	1.9	45°	30°	1.4
LSR	1.4	1.1	1.2	56°	31°	2.6
"	3.0	1.1	1.2	56°	31°	1.3
"	3.0	1.6	1.2	56°	31°	1.3
"	3.0	1.1	1.2	56°	31°	3.5
"	3.0	1.1	1.2	56°	31°	0.0

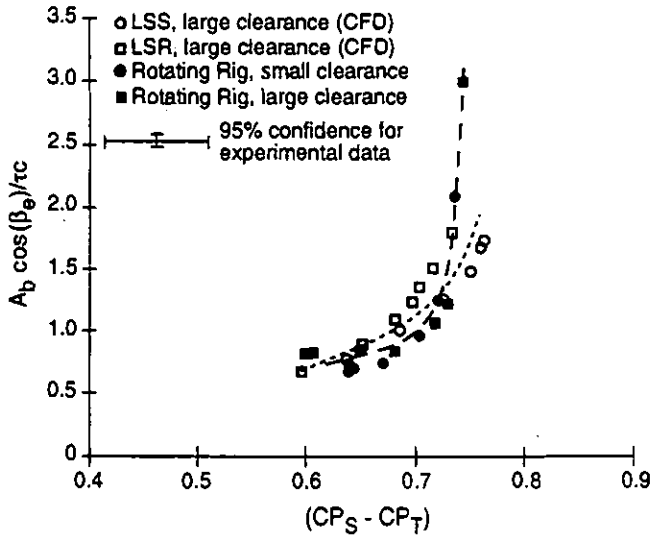

Figure 12: Comparison between CFD and experiment.

In Fig. 12 the rotor computations are compared to the rotating rig tests. At low loadings, the experimental blockage trends and computed results agree within the experimental error. More importantly, the limiting values of loading parameter between the two data sets are very close, differing by only 3% of the inlet dynamic head. The agreement of limiting loading parameter with experimental data suggests that the CFD solutions can be a useful tool to explore the parameter space of the endwall blockage problem and to examine the conditions at which the rapid rise in blockage occurs.

4.4 Summary of Experimental Data and Numerical Simulations

The experimental data and numerical simulations examined above cover a range of geometric parameters and flow conditions of practical interest. Over this range, there is a clear and consistent parametric trend of blockage variation with the loading parameter $CP_S - CP_T$, seen in the compressor and wind tunnel experiments as well as the computations. This implies not only that the computations can be used to assess these trends but that the overall ideas are not dependent on specific geometries and the basic physical idea is sound. From this basis, we can construct a simplified model to show the key design parameters that affect blockage, to give insight into the factors that determine its magnitude in a given flow condition, and to provide guidance for developing approaches to reduce or control blockage.

5.0 SIMPLIFIED ENDWALL BLOCKAGE CALCULATION PROCEDURE

If, as is argued here, the endwall blockage at the exit of a

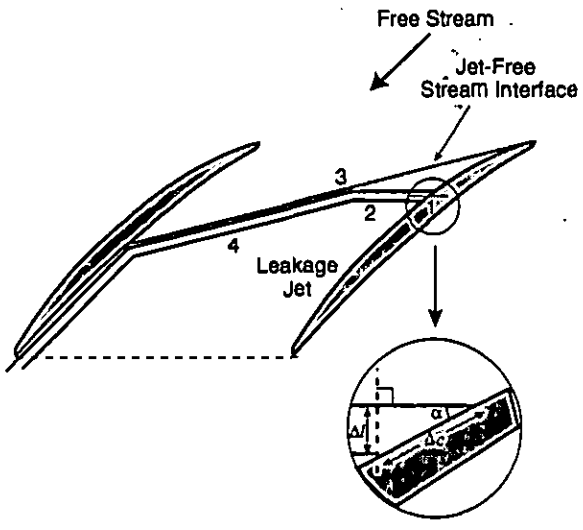

Figure 13: Radial view illustrating two-dimensional wake segments along the chord.

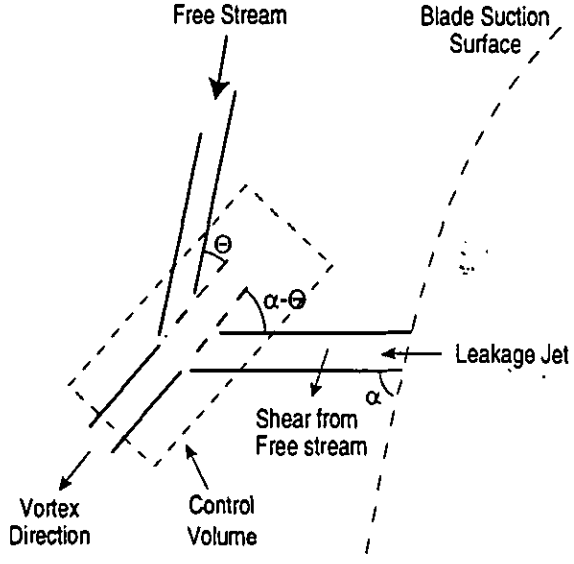

Figure 14: Jet-freestream interaction control volume.

compressor row can be viewed as similar to the growth of a velocity defect in an adverse pressure gradient, computation of this growth requires estimates of: (1) the initial velocity defect depth and extent, (2) the pressure gradient, and (3) the rate of mixing between defect and freestream (a feature not included in the 1-D analysis of Section 3). The complexity of the compressor endwall flow field offers many possible approximations for these flow processes, and the approach developed here is only one possible implementation. As will be shown, however, the procedure captures the experimentally observed parametric trends.

We make two assumptions to relate the actual process to the basic velocity defect description. First, the blockage at the passage exit is taken to be the summation of the blockage due to elemental regions of velocity defect which are created along the blade chord; in other words, each chordwise section of the leakage jet is assumed independent of the other sections. Second, the mixing and pressure rise are treated as if they occur sequentially. The framework for describing the endwall flow field is detailed below and shown schematically in Figure 13:

1. Fluid passes over the blade tip at a known leakage angle and total pressure for each section of the leakage jet. The leakage angle and total pressure can be taken directly from the computations or from a model such as that of Storer and Cumpsty (1991). At each chordwise location a single value, based on the mass average, is used.
2. Each chordwise segment of the leakage jet is taken to travel in a straight line, set by the leakage angle, until either reaching the jet/freestream interaction region or the passage exit. Shear layer mixing occurs at the interface between the jet and the freestream.
3. A control volume analysis is used to describe the interaction of the jet and the freestream, as shown in Fig. 14. The freestream velocity vector is assumed to follow the stagger angle of the blade. Conservation of mass and conservation of momentum in a direction parallel to and normal to the resultant vortex direction yield three equations for the angle of the vortex direction, the width, and the depth of the velocity defect (Martinez-Sanchez and Gauthier, 1990). The diminution in total pressure thus calculated provides the initial conditions for the velocity defect to pass through the adverse pressure gradient.
4. The defect growth downstream from the interaction is computed using a two-dimensional integral wake analysis (Hill *et al.*, 1963). In the present application, the defect is assumed to grow in the radial direction only.

Estimates of the errors introduced by the various assumptions

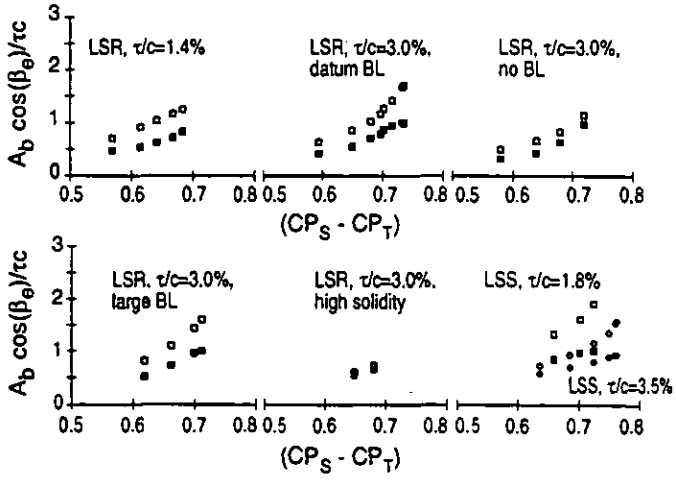

Figure 15: Normalized blockage versus loading parameter from CFD solutions and from blockage model: ❑ CFD results, ■ model.

associated with this description are outlined in Appendix A.

Computed values of blockage using the procedure described above are compared in Fig. 15 to the CFD solutions described in Table 2. The average difference between the blockages computed using the model and those obtained directly from the Navier-Stokes solutions is 33%, with a maximum difference of 46% for the high loading, low speed stator case. However, the predictions of absolute values of blockage differ in a systematic manner from the computations so that the parametric trends of endwall blockage for the range of clearances, boundary layer conditions and loadings investigated are, in fact, accurately predicted. This is shown in Figure 16, which shows the blockage normalized by the blockage at $(CP_S - CP_T)$ of 0.65. The calculation procedure captures the blockage versus loading trend for the low speed rotor cases with an average error of 5.5%, and those for the low speed stator with an average error of 12%.

6.0 PARAMETRIC TRENDS OF ENDWALL BLOCKAGE

Results from the numerical and experimental studies previously described were used together with the blockage model to provide quantitative information about the impact of design parameters and flow conditions on endwall blockage. The cases examined include inlet boundary layer thicknesses between zero and 3.5 clearance heights, blade stagger angles between 35 and 65 degrees, clearances between 1.4 and 3.5% of chord, solidities of 1.1 and 1.6, and jet total pressure coefficients equal to the free stream and to 60% greater than the free stream. As stated, while the model provides a rapid estimation of blockage, and thus could be used for example in design trade studies, its primary role is seen as providing insight into the relevant physical effects that set compressor endwall blockage.

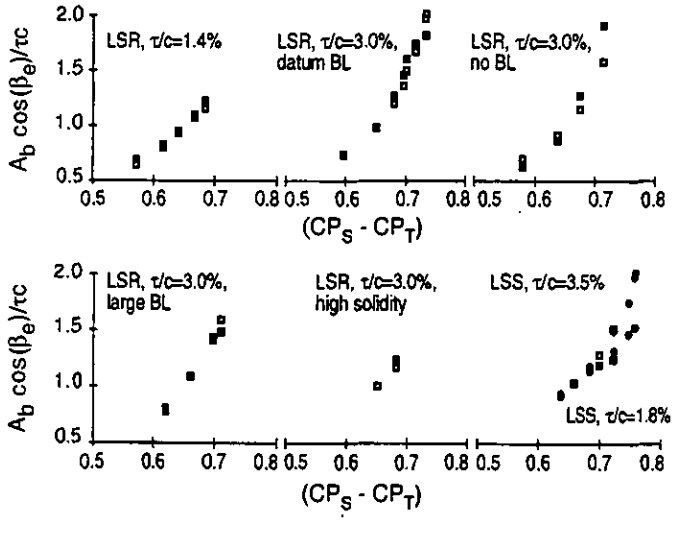

Figure 16: Blockage normalized by blockage at CP_S-CP_T = 0.65 versus loading parameter: ❑ CFD results, ■ model.

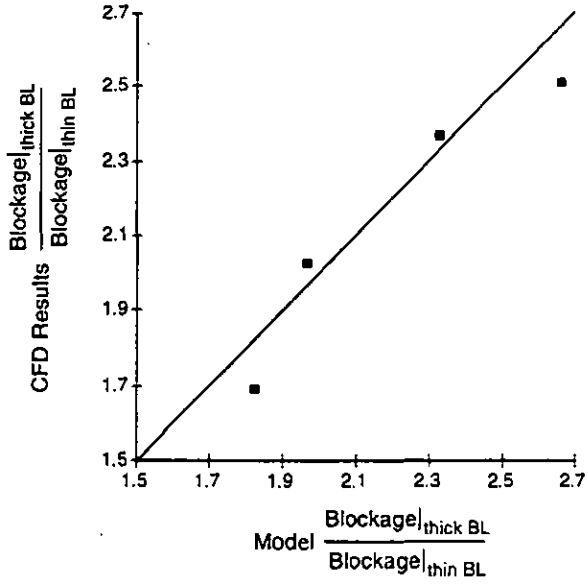

Figure 17: Effects of inlet boundary layer: ratio of blockages from thick (δ^*/t = 3.5) and thin (δ^*/t = 0.0) inlet boundary layer cases, computational solutions and model.

6.1 Inlet Boundary Layer

To examine the effect of inlet boundary layers on endwall blockage, computations were carried out for three different inlet boundary layer thicknesses. Cumpsty (1989) indicated that typical values of inlet boundary layer displacement thicknesses in axial compressors range from approximately one to three clearance heights, and the cases studied, $\delta^* = 0$ (no inlet boundary layer), $\delta^* = 1.3$ clearance heights (considered the datum case), and $\delta^* = 3.5$ clearance heights, bound this range.

The trends provided by the blockage model are shown in Fig. 17, which gives the ratio of blockages between the thick and thin inlet boundary layer cases for the CFD and the model calculations. Agreement is within 7%. For the same value of the loading parameter, the normalized blockage increased from approximately 0.8 of the datum value to 1.2 of the datum value as the inlet displacement thickness changed from 0 to 3.5 clearance heights. The physical reason for the increase is that the inlet boundary layer affects the clearance jet total pressure, and hence the depth of the initial velocity defect, resulting in a lower limiting static pressure rise for a thicker inlet boundary layer. The stalling static pressure rise coefficient was 4% higher for no inlet boundary layer compared to the thick inlet boundary layer.

6.2 Clearance Height

The effects of clearance size on endwall blockage were given in Fig. 12, where results from the rotating rig and the rotor computations were presented. The blockage values in this figure are shown normalized by the clearance area (τc). Comparing the experimental data for the large clearance to that for the small clearance, and the computations for the large and small clear-

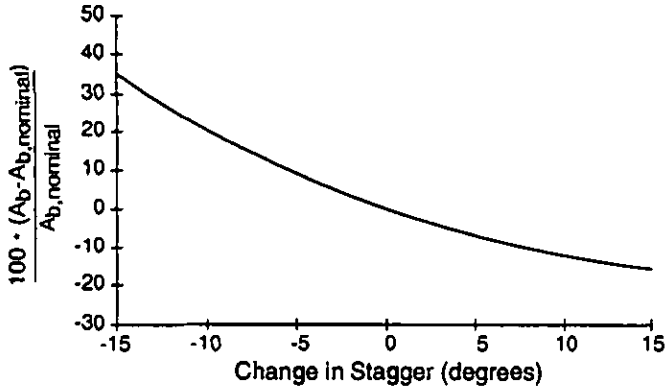

Figure 18: Predicted changes in blockage with changes in stagger angle for an initial stagger angle of 45°, $\Delta P/Q = 0.5$, $\sigma = 1.1$, τc = constant.

ance, shows less than 20% difference in normalized blockage across the entire speedline. The data indicate, therefore, that endwall blockage is approximately proportional to clearance height; thus doubling the clearance size will approximately double the exit plane blockage. The results from the blockage model shown in Fig. 15 are in accord with this conclusion, a 5% increase in normalized blockage for a two-fold increase in clearance height. Note, however, that for tight clearances, say below 1% of chord, Khalid (1995) and Storer and Cumpsty (1991) show that endwall performance is increasingly affected by three-dimensional separation in the endwall-suction side corner and the mechanism for increased blockage with loading will be quite different.

6.3 Stagger Angle

The effect of stagger angle variation on blockage is presented in Fig. 18. The figure shows the percent change in blockage ($A_{b,nominal}$ is the blockage at the initial stagger angle) versus changes in stagger angle for an initial stagger angle of 45°. For the cases shown, the non-dimensional solidity is 1.1 and the clearance area, τc, is held constant as stagger changes. The model shows that, as stagger is increased, both the clearance mass flux and the clearance leakage angle decrease. The result of these two effects is a reduction in the exit plane blockage as stagger angle is increased.

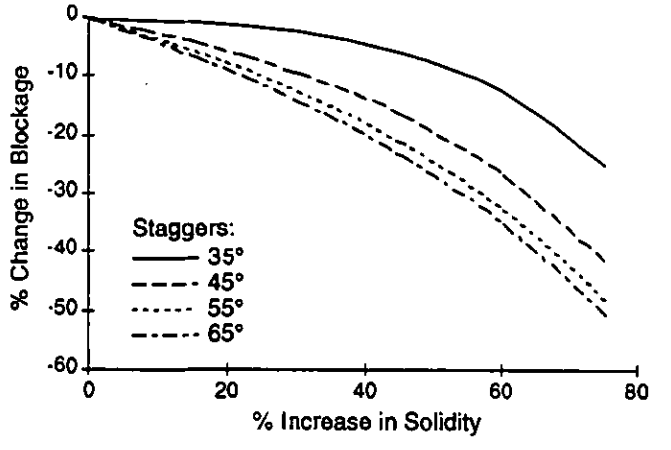

Figure 19: Predicted changes in blockage with changes in solidity for $\Delta P/Q = 0.5$, initial solidity=1.1, and various initial stagger angles.

6.4 Solidity

Modeled changes in blockage with increasing solidity are shown in Fig. 19 for stagger angles ranging from 35° to 65°. The cases shown are for a non-dimensional pressure $\Delta P/Q$ of 0.5 and an initial solidity of 1.1. For a 50% increase in solidity, blockage is reduced by 5% to 30% for stagger angles ranging from 35° to 65°, respectively.

This is because increasing the solidity decreases the blade loading for the same overall passage pressure rise, reducing the leakage jet angle and the clearance mass flux. The result is a leakage jet with an effectively higher initial total pressure and hence a reduced normalized blockage. For cases in which the tip leakage vortex trajectory intersects the next blade pressure surface, an increase in solidity results in an increase in double leakage (described in Appendix A), increasing clearance jet loss, and partially offseting the blockage reduction caused by the decreased blade loading.

6.5 Blade Loading Profile

The effect of blade loading profiles can be seen by comparing the blockage trends of the low speed rotor, the low speed stator, and the Deverson rotor. The different pressure distributions for these three cases caused different distributions of leakage velocity (computed using the procedure developed by Storer and Cumpsty (1991)) along the chord as shown in Fig. 20, but the blockage trends for all three are similar. The implication is

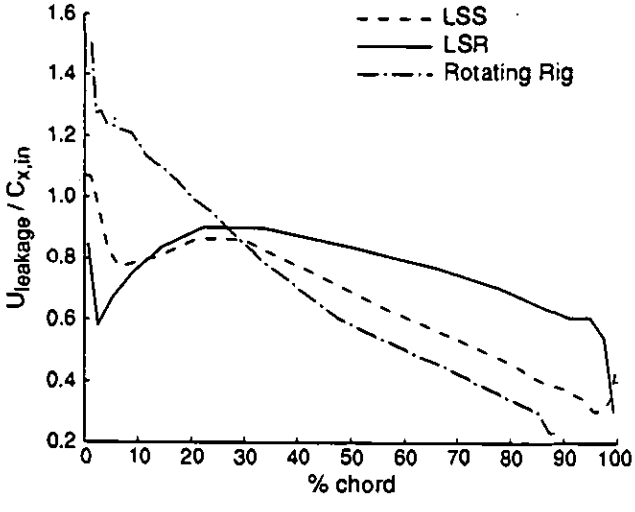

Figure 20: Leakage velocity versus chord for low speed stator, low speed rotor, and Deverson rig tests.

and Cumpsty (1991)) along the chord as shown in Fig. 20, but the blockage trends for all three are similar. The implication is that the details of the loading profile are not a major factor in determining endwall blockage trends. Storer and Cumpsty have also argued this point, based on analysis of circular and parabolic arc camber line cascades. Unless one considers blade designs that reduce the chord-averaged blade loading near the tip for the same passage pressure rise, it is expected that blade loading profile will not be a large factor in determining endwall blockage. To produce a 50% reduction in exit plane endwall blockage, the required reductions in the loading parameter near the tip were estimated to be 74%. This suggests that using three-dimensional blade designs to reduce blade tip loading and hence endwall blockage may be difficult.

.6 Increased Clearance Jet Total Pressure

technique often used for controlling endwall flow is casing treatment. It has been shown that one of the features of casing treatment is an increased total pressure in the leakage jet. he effect of this high total pressure fluid on endwall blockage as quantified using the wind tunnel and the blockage prediction method. In the wind tunnel two levels of increased jet total ressure ($CP_{T,jet}$ = 0.6 and 0.3) were tested over two different hordwise extents (25% and 50% of chord). The total pressure oefficient profiles, which were based on Navier-Stokes modeling of a blade row with casing treatment (see Khalsa, 1996), were reated in the wind tunnel described in Section 4.2 using different solidity screens placed behind the jet injector.

igure 21 shows the measured changes in blockage for various loading conditions and levels of clearance jet total pressure. or a given location, the higher the total pressure, the larger the eduction in blockage. At a given jet total pressure level, a heightened clearance jet total pressure over the first 50% of the chord yielded only a 10 to 15% improvement compared to high total

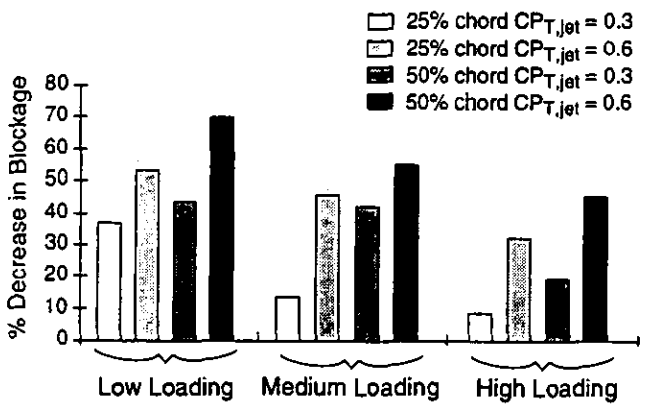

Figure 21: Measured reduction in blockage due to high total pressure jet. Data obtained from wind tunnel measurements.

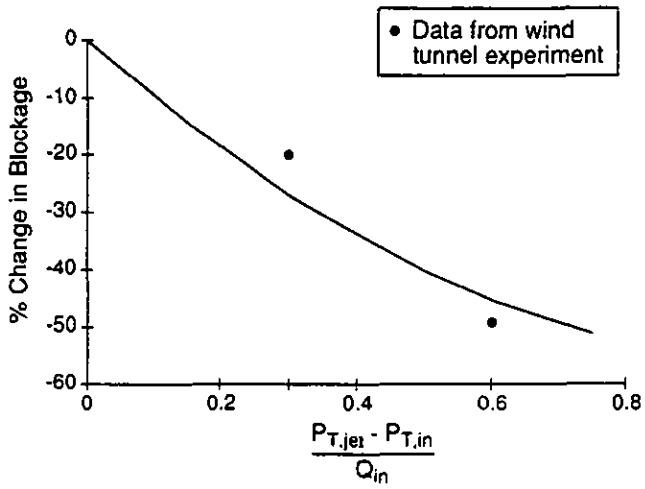

Figure 22: Modeled reduction in blockage when jet total pressure is increased over the front 50% of the chord.

pressure over the upstream 25% of the chord. Near stall, increased jet total pressure reduced blockage approximately 20% less than for the low loading cases.

The blockage reduction due to increasing the jet total pressure was also estimated using the simplifed blockage model. Cases were calculated with increased clearance jet total pressure coefficient over the front 50% of the clearance jet. The blockage reduction calculated is shown in Fig. 22 which shows that a 60% increase in jet total pressure would result in a 45% reduction in blockage. This result is in good agreement to the experiments which indicate a 49% reduction in blockage for the same level of blowing at near-stall conditions.

.0 SUMMARY AND CONCLUSIONS

) new methodology for quantifying compressor endwall lockage has been developed. The approach, which can be regarded as adapting the concept of displacement thickness to the hree-dimensional flows found in compressors, provides a clear etric for evaluating the effect of endwall flow on pressure rise apability.

) omputations and experiments have been examined in light f this blockage definition. The results suggest a parameter set hich collapses the experimental and numerical data for endwall lockage onto a single trend line for all situations assessed.

) simplified analysis has been developed which enables estimation of endwall blockage with good accuracy (trends captured to better than 10%). An additional, and potentially more mportant application of this tool is that it can provide physical nsight into the interacting fluid dynamic processes involved in learance related blockage generation.

) he simplified analysis is based on a view of the blockage s due to the growth of the region of low total pressure fluid ssociated with the tip leakage, with the behavior roughly simil-

5) A wind tunnel simulation for the tip leakage flow has been developed. The results from the tunnel experiments, which agree with rotating rig measurements of blockage to better than 10%, provide information on the variation in blockage with leakage flow angles and clearance total pressure, the latter being a key feature of casing treatment operation.

8.0 REFERENCES

Adamczyk, J. J., Celestina, M. L., Beach T. A., and Barnett, M., 1989, "Simulation of Three-Dimensional Viscous Flow within a Multistage Turbine," *ASME Journal of Turbomachinery*, Vol. 112, pp. 370-376.

Baldwin, B. and Lomax, H., 1978, "Thin Layer Approximation and Algebraic Model for Separated Turbulent Flows," AIAA Paper No. 78-257.

Crook, A.J., Greitzer, E.M., Tan, C.S., Adamczyk, J.J., 1993, "Numerical Simulation of Compressor Endwall and Casing Treatment Flow Phenomena," *ASME J. of Turbomachinery*, Vol. 115, pp. 501-512.

Cumpsty, N. A., 1989, *Compressor Aerodynamics*, Longman Scientific and Technical Publications.

Dring, R.P., 1984, "Blockage in Axial Compressors," *ASME J. of Eng. for Gas Turbines and Power*, Vol. 106, No. 3, pp. 712-714.

Hill, P. G., Schaub, U. W., and Senoo, Y., 1963, "Turbulent Wakes in Pressure Gradients," *Trans. ASME*, pp. 518-524.

Horlock, J. H. and Greitzer, E. M., 1983, "Non-Uniform Flows in Axial Compressors due to Tip Clearance Variation," *Proc. Instn. Mech. Engrs.*, Vol 197C, pp. 173-178.

Johnson, M. C., Greitzer, E.M., 1987, "Effects of Slotted Hub and Casing Treatments on Compressor Endwall Flowfields," *ASME J. Turbomachinery*, Vol. 109, pp. 380-387.

Khalid, S. A., 1995, "The Effects of Tip Clearance on Axial Compressor Pressure Rise," internal Gas Turbine Laboratory Report.

Khalsa, A. S., 1996. "Endwall Blockage in Axail Compressors," Ph.D. thesis, Department of Aeronautics and Astronautics, Massachusetts Institute of Technology.

Kirtley, K. R., Beach, T. A., and Adamczyk, J. J., 1990, "Numerical Analysis of Secondary Flow in a Two-Stage Turbine," AIAA Paper No. 90-2356.

Koch, C.C., 1981, "Stalling Pressure Rise Capability of Axial Flow Compressor Stages," *ASME J. of Eng. for Power*, Vol. 103, pp. 645-656.

Martinez-Sanchez, M. and Gauthier, R. P., 1990, "Blade Scale Effects of Tip Leakage," Gas Turbine Laboratory Report #202. .

Rediniotis, O. K., Hoang, N. T., and Telionis, D. P., 1993, "The Seven-Hole Probe: Its Calibration and Use," FED-Vol 152, Instructional Fluid Dynamic Experiments, pp. 21-26.

Schweitzer, J.K., Garberoglio, J.E., 1984, "Maximum Loading Capability of Axial Flow Compressors," *J. Aircraft*, Vol. 21, No. 8, pp. 593-600.

Smith, G. D. J. and Cumpsty, N. A., 1984, "Flow Phenomena in Compressor Casing Treatment," ASME Journal of Engineering for Gas Turbines and Power, Vol. 106, No. 3, pp 532-541.

Smith, L.H., Jr., 1970, "Casing Boundary Layers in Multistage Axial-Flow Compressors," *Flow Research in Blading*, L.S. Dzung, Ed., Elsevier, Amsterdam.

Storer, J.A., Cumpsty, N.A., 1991, "Tip Leakage Flow in Axial Compresors," *J. of Turbomachinery*, Vol. 113, pp. 252-259.

Strazisar, A.J., Wood, J.R., Hathaway, M.D., Suder, K.L., 1989, "Laser Anemometer Measurements in a Transonic Axial-Flow Fan Rotor," NASA TP-2879.

Suder, K., 1997, "Blockage Development in a Transonic, Axial Compressor Rotor," ASME 97-GT-394.

Wisler, D. C., 1977, "Core Compressor Exit Stage Study, Volume I - Blading Design," NASA CR-135391.

Wisler, D. C., 1981, "Core Compressor Exit Stage Study, Volume IV - Data and Performance Report for the Best Stage Configuration," NASA CR-165357.

Wisler, D.C., 1985, "Aerodynamic Effects of Tip Clearance, Shrouds, Leakage Flow, Casing Treatment and Trenching in Compressor Design," Von Karman Institute Lecture Series 1985-05 on Tip Clearance Effects in Axial Turbomachinery.

APPENDIX A: ASSESSMENT OF PRIMARY ASSUMPTIONS USED IN BLOCKAGE ESTIMATION PROCEDURE

The assumption which causes the largest error in the simplified blockage calculation method is that the static pressure change from the jet-freestream interface to the passage exit can be approximated by the static pressure change from the blade surface to the passage exit. This assumption was determined to cause up to a 38% underprediction of blockage.

A second assumption is that the leakage jet experiences no pressure change between the blade suction surface and the jet-freestream interaction region. This assumption was tested by

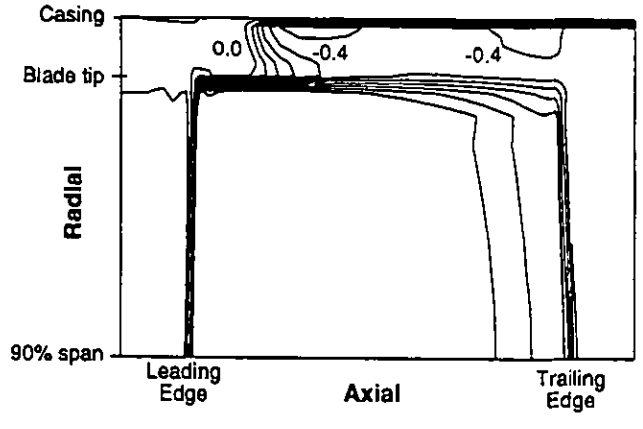

Figure A.1: Total pressure coefficient at clearance gap exit, τ/c = 3%, near stall.

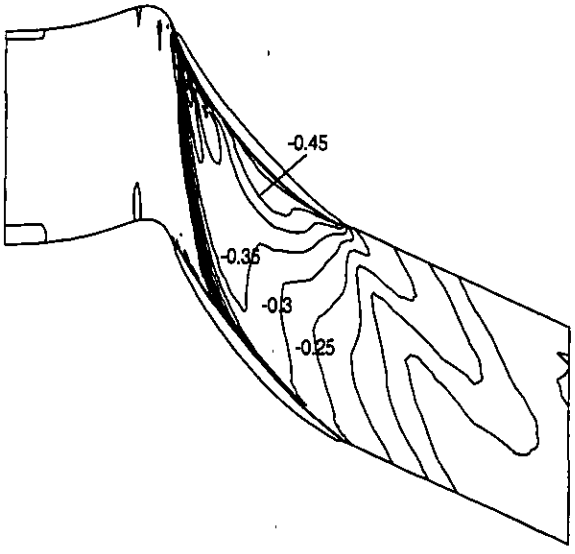

Figure A.2: Total pressure coefficient contours at blade tip radius, near stall.

examining representative streamlines in the CFD solutions. The results suggest that this assumption is responsible for less than 10% under-calculation of exit-plane blockage.

An assumption not examined is whether the mixing of the defect between the jet-freestream interface and the passage exit occurs in a manner similar to a two-dimensional wake. The validity of this assumption perhaps can be inferred by the agreement between the model and data.

To accurately predict the clearance jet leakage angle, the total pressure of the fluid exiting the clearance gap must be known. Storer and Cumpsty (1991) assumed that the total pressure of the leakage jet is equal to the freestream total pressure, which was not valid for some of the cases examined for this paper. Figure A.1 shows a tangential view of the total pressure field in the clearance of the low speed rotor. The total pressure coefficient over the rear 60% of chord was below -0.4. The cause of this reduction in clearance jet total pressure can be seen in plots of total pressure coefficient in an axial-tangential plane at the blade tip radius, shown in Fig. A.2. The leakage flow is transported across the passage to the pressure side of the adjacent blade. This results in a reduction in the total pressure of the fluid at the entrance to the adjacent clearance gap between 40% chord and the blade trailing edge.

When fluid from the leakage jet passes under a second blade in this manner, the total pressure of the clearance jet is reduced, lowering the leakage angle. If this reduction in leakage angle is not taken account of in the blockage calculation procedure, the calculated blockage can be as much as 30% too high. The calculations presented here used the CFD results to supply the leakage jet total pressure, primarily to avoid this source of error.

A second error that double leakage introduces into these calculations is associated with the assumption that all fluid leaking over the blade tip contributes to that passage's exit plane blockage. However, fluid that passes into any adjacent passage can not contribute to exit plane blockage of the passage in which it originated. The CFD calculations indicate an upper bound for this error is approximately 20% overprediction of blockage using the simplified calculation procedure.

A balance between the errors due to neglecting double leakage (causing the calculated blockage to be too high) and due to the pressure gradient assumptions (causing the calculated blockage to be too low) provides a likely explanation for the more accurate calculation of blockage at increased solidity than at nominal solidity. For similar passage loading, the increased solidity geometries have more double leakage than the one with nominal solidity and hence a larger overprediction error due to neglecting the double leakage.